2011

Surface charging at the (1 0 0) surface of Cu doped and undoped Li2B4O7

Jie Xiao

N. Lozova

Ya. B. Losovyj

D. Wooten

I. Ketsman

See next page for additional authors

Authors

Jie Xiao, N. Lozova, Ya. B. Losovyj, D. Wooten, I. Ketsman, M. W. Swinney, J. Petrosky, J. McClory, Ya. V. Burak, V. T. Adamiv, A. T. Brant, and P. A. Dowben

Applied Surface Science 257 (2011) 3399–3403

Contents lists available at ScienceDirect

Applied Surface Science

journal homepage: www.elsevier.com/locate/apsusc

Surface charging at the (1 0 0) surface of Cu doped and undoped $Li_2B_4O_7$

Jie Xiao[a], N. Lozova[b], Ya.B. Losovyj[a,b], D. Wooten[c], I. Ketsman[a], M.W. Swinney[c], J. Petrosky[c], J. McClory[c], Ya.V. Burak[d], V.T. Adamiv[d], A.T. Brant[e], P.A. Dowben[a,*]

[a] Department of Physics and Astronomy and the Nebraska Center for Materials and Nanoscience, University of Nebraska-Lincoln, Theodore Jorgensen Hall 855 North 16th Street, Lincoln, NE 68588-0299, USA
[b] J. Bennett Johnston Sr. Center for Advanced Microstructures and Devices, Louisiana State University, 6980 Jefferson Highway, Baton Rouge, LA 70806, USA
[c] Air Force Institute of Technology, 2950 Hobson Way, Wright Patterson Air Force Base, OH 45433-7765, USA
[d] Institute of Physical Optics, 23 Dragomanov Str., Lviv 79005, Ukraine
[e] Department of Engineering Physics, West Virginia University, Morgantown, WV 26506, USA

ARTICLE INFO

Article history:
Received 19 March 2010
Received in revised form 3 November 2010
Accepted 4 November 2010
Available online 16 November 2010

PACS:
79.60.Ai
68.55.Ln
29.40.Wk
81.05.J

Keywords:
Oxide dielectric layers
Lithium borate
Surface photovoltaic charging

ABSTRACT

We have compared the photovoltaic charging of the (1 0 0) surface termination for Cu doped and undoped $Li_2B_4O_7$. While the surface charging at the (1 0 0) surface of $Li_2B_4O_7$ is significantly greater than observed at (1 1 0) surface, the Cu doping plays a role in reducing the surface photovoltage effects. With Cu doping of $Li_2B_4O_7$, the surface photovoltaic charging is much diminished at the (1 0 0) surface. The density of states observed with combined photoemission and inverse photoemission remains similar to that observed for the undoped material, except in the vicinity of the conduction band edge.

1. Introduction

With the fabrication of a semiconducting boron carbide, a material suitable for the fabrication of solid state neutron detectors [1–7], there has been a resurgence in the development of boron based semiconductors for neutron detection. In addition to the boron carbides [1–7], possible boron based semiconductors for solid state neutron detectors include boron nitrides [8,9], boron phosphides [10–11], and the lithium borates [12,13]. Although $Li_2B_4O_7$ lithium borate has a much larger (6.3–10.1 eV) band gap [14–20] than the boron carbides, boron nitrides, or boron phosphides, this class of materials has distinct advantages. Because of the large band gap, lithium borates are typically transparent in the range of 165–6000 nm and furthermore can be isotopically enriched to a high degree. $Li_2B_4O_7$ can be isotopically enriched to 95 at% ^{6}Li and 97.3 at% ^{10}B [13] from the natural 7.4 at% ^{6}Li and 19 at% ^{10}B.

Since lithium tetraborate ($Li_2B_4O_7$) single crystals are pyroelectric and piezoelectric [19–22], surface termination and interface effects must be seriously considered in solid state device design. This is a critical consideration as doping will serve to enhance differences along different crystal directions [23]. Doping of the $Li_2B_4O_7$ is certainly possible [13], and essential for solid state neutron detection applications, given the very high resistivities of undoped crystals. The undoped $Li_2B_4O_7$ resistivities are on the order of 10^{10} Ω cm [12], so that doping is essential to both suppress pyroelectricity and increase transport, ideally electron transport as the hole mass is quite large as indicated by the band structure [18,20]. In fact, Cu doping is indeed seen to increase carrier lifetimes [20,24], further indicating the importance of doping for device applications [20].

2. Experimental

The $Li_2B_4O_7$ and $Li_2B_4O_7$:Cu single crystals, both with the natural isotope distribution (^{6}Li – 7.4%, ^{7}Li – 92.6%, ^{10}B – 19% and ^{11}B – 81%), were grown from the melt by the Czochralski technique as described elsewhere [13,15,16]. The Cu dopant centers are seen to be univalent Cu^+ ions in the $Li_2B_4O_7$ lattice, inde-

* Corresponding author. Tel.: +1 402 472 9838; fax: +1 402 472 2879.
E-mail address: pdowben@unl.edu (P.A. Dowben).

0169-4332/$ – see front matter © 2010 Elsevier B.V. All rights reserved.
doi:10.1016/j.apsusc.2010.11.033

pendent of the valence of Cu in the initial chemical agent used for doping. We doped $Li_2B_4O_7$ single crystals using CuO in the growth mixture, as was done previously [17,25]. The distribution coefficient depends on Cu concentration in the melt, but does not exceed 0.04, and the single crystal $Li_2B_4O_7$:Cu doped samples are nominally $Li_{1.998}Cu_{0.002}B_4O_7$, as determined by quantitative spectrographic analysis. Clean surfaces were prepared by several methods including resistive heating and combinations of sputtering and subsequent annealing. The electronic structure and stoichiometry were similar in all cases [18,19].

Combined ultraviolet photoemission (UPS) and inverse photoemission (IPES) spectra were used to characterize the placement of both occupied and unoccupied states in $Li_2B_4O_7$ single crystals at the (1 0 0) and (1 1 0) surfaces. The temperature-dependent angle-resolved photoemission experiments were performed using the 3 m toroidal grating monochromator (3 m TGM) beam line [26] in an ultra high vacuum (UHV) chamber previously described [18–19,26–28]. Photoemission was conducted over a range of temperatures from 250 to 700 K. Throughout this work, the light incidence angle was 45° but changes were made to the direction of the in-plane component orientation of the **E** of the plane-polarized incident light. The photoelectrons were collected along the surface normal throughout this work to preserve the high point group symmetry ($\overline{\Gamma}$).

The inverse photoemission (IPES) spectra were obtained by using variable energy electrons incident along the sample surface normal, again to preserve the high point group symmetry ($\overline{\Gamma}$), while measuring the emitted photons at a fixed energy (9.7 eV) using a Geiger-Müller detector with an instrumental linewidth of about 400 meV [18,19,29–30]. The inverse photoemission spectra were taken for sample temperatures of 300–400 K, but no surface charging was observed in the inverse photoemission. Checks to the placement of the Fermi level in both the angle-resolved photoemission and inverse photoemission experiments were performed using tantalum films in electrical contact with the samples. Surface charging shifts in the photoemission were also taken into account by using the Li 1s and O 2s shallow core levels as reference energy levels [19,31].

A Bruker EMX spectrometer operating near 9.48 GHz was used to take EPR data. A helium-gas-flow system maintained the sample temperature near 20 K, and a proton NMR gaussmeter provided values of the static magnetic field. A small Cr-doped MgO crystal was used to correct for the difference in magnetic field between the sample and the probe tips of the gaussmeter (the isotropic g value for Cr^{3+} in MgO is 1.9800). An X-ray tube (operating at 60 kV and 30 mA) was used to convert defects in the $Li_2B_4O_7$ crystals to their paramagnetic charge states. Irradiation times were 30 min.

3. The $Li_2B_4O_7$(1 0 0) valence and conduction band density of states

From Fig. 1, it is clear that for the nominally undoped $Li_2B_4O_7$(1 0 0), the band gaps obtained from combined photoemission and inverse photoemission are 10.1 ± 0.5 eV and 8.9 ± 0.5 eV at the high symmetry $\overline{\Gamma}$ point of each surface, with the in plane component of **E** aligned along the [0 1 1] and [0 1 0] directions, respectively. This tends to be towards the higher end of the theoretically predicted band gaps that range from 6.2 to 9.7 eV [14–16]. This value determined from the combined photoemission and inverse photoemission is also somewhat larger than the value of 7.4–7.5 eV estimated from the optical absorption edge [17], as expected for photo-excitations due to Coulomb interactions with the photohole. This band gap value, determined from the combined photoemission and inverse photoemission, is in surprisingly good agreement with LDA calculations [14], given that local density approximation (LDA) models will typically underestimate the band gap [32–37]. The experimental estimate of the band gap could also be flawed for several reasons: the data is shown for only a limited wave vector sample (not averaged for the entire bulk Brillouin zone) and charging effects that remain (not removed in the binding energy corrections to the data [18], in Fermi level placement calibrations) will tend to increase the apparent band gap. Furthermore photoemission and inverse photoemission are final state [38], not initial state spectroscopies, and very surface sensitive.

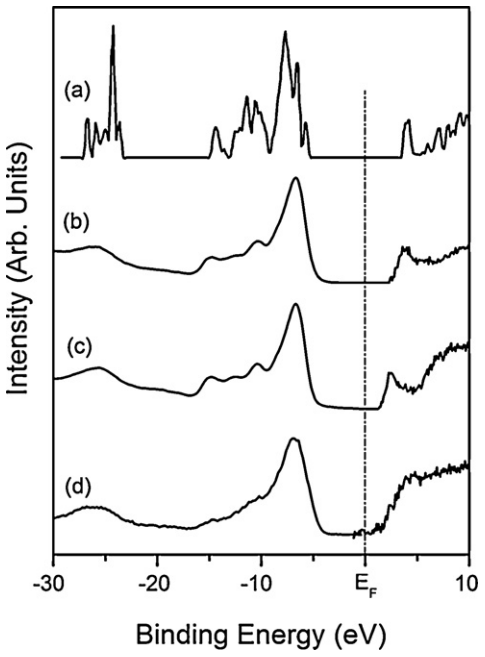

Fig. 1. A comparison of the combined experimental photoemission (left) and inverse photoemission (right) data, in $E - E_F$, with theoretical expectations. The theoretical density of the bulk band states of crystalline $Li_2B_4O_7$ (a) obtained by the LDA PW1PW is adapted from Islam et al. [14]. The combined experimental photoemission (left) and inverse photoemission (right) data for $Li_2B_4O_7$(1 0 0), with the in-plane component of the incident light **E** for photoemission oriented along [0 1 1] (b) and [0 1 0] (c) are shown along with the data for Cu doped $Li_2B_4O_7$(1 0 0) surface (d). For the photoemission, the synchrotron light is incident at 45° with respect to surface normal. The electrons were either collected along the surface normal (photoemission) or incident along the surface normal (inverse photoemission).

In spite of the numerous deficiencies of the combined photoemission and inverse photoemission experiments, as shown previously [18], the $Li_2B_4O_7$(1 0 0) surface exhibits a density of states that qualitatively resembles that expected from the model bulk band structure of $Li_2B_4O_7$ [14–16], as seen in Fig. 1. Surface contributions, nonetheless, cannot be neglected, and there is now much evidence in support of surface states at the surface of $Li_2B_4O_7$(1 1 0) [18,31]. The Fermi level is placed slightly closer to the conduction band edge in the combined experimental photoemission and inverse photoemission spectra, as seen in Fig. 1. This indicates that the $Li_2B_4O_7$(1 0 0) surfaces are n-type [18]. While we have not measured the majority carrier, the Fermi level placement is consistent with the known bulk properties where the majority of defects seen in nominally undoped $Li_2B_4O_7$(1 0 0) and $Li_2B_4O_7$(1 1 0) were oxygen vacancies [39].

4. The effect of Cu doping of $Li_2B_4O_7$

Electron paramagnetic resonance (EPR) and electron-nuclear double resonance (ENDOR) techniques are well suited to identify and characterize paramagnetic point defects in bulk crystals such as $Li_2B_4O_7$ [39]. Information from hyperfine interactions is especially useful in developing specific models for point defects [39]. Gen-

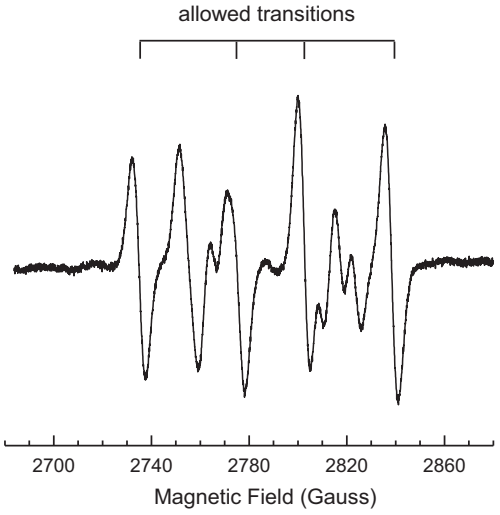

Fig. 2. EPR spectrum of Cu^{2+} ions substituting for lithium in a nominally undoped $Li_2B_4O_7$ crystal with a total defect density approximately 5 ppm or less. These data were taken at 20 K with the magnetic field along the [0 0 1] direction. A large nuclear electric quadrupole interaction is responsible for the asymmetric appearance of the spectrum.

erally, EPR studies in $Li_2B_4O_7$ have focused on Cu^+ [16,25,39,40], Co^{2+} and Mn^{2+} [41–42], impurities substituting for lithium and vacancy-related defects produced by neutron irradiation at room temperature. The Cu impurity centers in the $Li_2B_4O_7$ lattice generally adopt the univalent Cu^{1+} ion state [17,25,40,43–46], independent of the valence of the initial chemical copper source additive agent used for Cu doping.

Fig. 2 shows the EPR spectrum of Cu^{2+} ions in the nominally undoped $Li_2B_4O_7$ crystal, where the copper impurities amount only a trace amount (much less than 5 ppm). This spectrum was taken at 20 K with the magnetic field along the [0 0 1] direction after the crystal was irradiated at 77 K with X-rays. All of the crystallographically equivalent copper sites are magnetically equivalent for this orientation of magnetic field. Copper impurity ions substitute for lithium ions in the $Li_2B_4O_7$ lattice [17,25,39,40,43–46], with most of them being in the monovalent charge state prior to the X-ray irradiation. Heating above room temperature restores the pre-irradiation distribution of copper charge states. Indeed, thermoluminescence data indicates that the recombination process $Cu^{2+} + e$ to $Cu^{1+} + h\nu$ occurs in the region of 362 K or less [25]. These ground state Cu^+ ($3d^{10}$) impurity ions convert to Cu^{2+} ($3d^9$) ions during the irradiation as they trap "free" holes from the valence band [39] or (alternatively) the electron of the Cu^{2+} exciton resides in the nearest appropriate lattice defect site [25]. The Cu impurities are extremely robust and stable in the 1+ state, even in the nominally $Li_{1.998}Cu_{0.002}B_4O_7$, both as grown [17,25,39–40,43–46] and after irradiation at room temperature with X-rays [17].

The effective g value for the Cu^{2+} spectrum in $Li_2B_4O_7$ is 2.4302 ($\pm$0.0003) when the magnetic field is along the [0 0 1] direction. A recent EPR angular dependence study by Corradi et al. [40] provides complete **g** and **A** matrices for these Cu^{2+} ions. Normally, an EPR spectrum from Cu^{2+} ions contains four equally spaced hyperfine lines due to the ^{63}Cu and ^{65}Cu isotopes. Both isotopes have $I = 3/2$ and their nuclear magnetic moments are similar (^{63}Cu is 69.2% abundant and ^{65}Cu is 30.8% abundant). In many cases, signals from the two isotopes are resolved and eight lines (two similar sets of four lines) are observed in the EPR spectrum. The hyperfine pattern in Fig. 2, however, does not resemble a simple four-line hyperfine pattern because nuclear electric quadrupole interactions produce shifts in the allowed line positions and also introduce "forbidden" lines. With the magnetic field along the [0 0 1] direction in Fig. 2, allowed lines are at 2735, 2775, 2803, and 2838 G and forbidden lines appear between the first and second and the third and fourth allowed lines. For directions of the magnetic field other than those near [0 0 1], nuclear electric quadrupole effects are not easily observed in the Cu^{2+} spectra from $Li_2B_4O_7$ crystals because the hyperfine term in the spin Hamiltonian becomes considerably larger than the nuclear quadrupole term.

Since copper is nominally divalent and occupies a lithium site, increasing the Cu impurities should increase the number of donor states or, alternatively, the number of hole trapping states in lithium tetraborate ($Li_2B_4O_7$). The former interpretation is consistent with the combined photoemission and inverse photoemission studies of doped and undoped $Li_2B_4O_7$(1 0 0) illustrated in Fig. 1. The conduction band edge is relatively sharp in the inverse photoemission for the nominally undoped $Li_2B_4O_7$(1 0 0) surfaces. By increasing the Cu doping concentration, the $Li_2B_4O_7$(1 0 0) conduction band edge becomes very gradual, tailing off to energies within 1–2 eV above the reference Fermi level. Because this is observed in inverse photoemission, this could well be a surface effect indicating an increase in surface oxygen vacancies, which would tend to make the surface more n-type. If band bending is excluded, it is also possible that the Cu atoms occupying the Li sites will also act as donor sites (as noted above) and a more heterogeneous distribution of donor sites would account for the more gradual increase in the conduction band edge density of state away from the Fermi level. If either the surface or bulk donor states density increases with Cu doping then the surface photovoltaic charging should diminish compared to the undoped $Li_2B_4O_7$(1 0 0) surfaces.

If the Cu impurities actually increase the number of hole traps, then, in spite of the heavy hole mass expected from the band structure [18], the resulting decrease in hole carrier mobilities should decrease the conductivity. There is also the possibility that the Cu^{1+} impurity ion traps an electron to go to a transient Cu^0 state, as suggested by the thermoluminescence [25] and cathodoluminescence [20,24,47] of $Li_2B_4O_7$:Cu. If either process occurs with appreciable probability at the surface as well, then the surface photovoltaic charging should increase compared to the undoped $Li_2B_4O_7$(1 0 0) surfaces. But the cathodoluminescence line widths, which will include a strong surface component, suggest that electron life-time is, in fact, much longer for the $Li_2B_4O_7$:Cu single crystals than the undoped $Li_2B_4O_7$ single crystals [20,24], giving rise to the very real possibility of an increase in surface and, possibly, bulk conductivity with copper doping possibly via both electrons and holes.

5. Surface photovoltaic charging

The recognition and use of surface photovoltage (SPV) was first implemented by Brattain and Bardeen in 1953 [48] and the technique has been subsequently much exploited [49] largely for semiconductors characterization. Surface photovoltage effects with temperature, substrate doping and metal deposition dependence [50–52] have provided a means by which phonon based recombination and Schottky barrier heights, due to metal induced gap states, can be observed and measured by ultraviolet photoemission spectroscopy. Fig. 3 shows the surface photovoltage charging, as observed in photoemission, for Cu doped $Li_2B_4O_7$(1 0 0). These photoemission spectra, with increasing then decreasing temperature, exhibit a temperature dependent shift in all of the photoemission features.

In Fig. 4, we have plotted the binding energies of the valence band maximum with temperature. The shift in the valence band maximum is much greater for $Li_2B_4O_7$(1 0 0) than for $Li_2B_4O_7$(1 1 0), but significantly reduced with Cu doping of $Li_2B_4O_7$(1 0 0). In many such cases, the surface voltaic charging can be dominated by surface conductivity. The decreased charging observed for the Cu doped

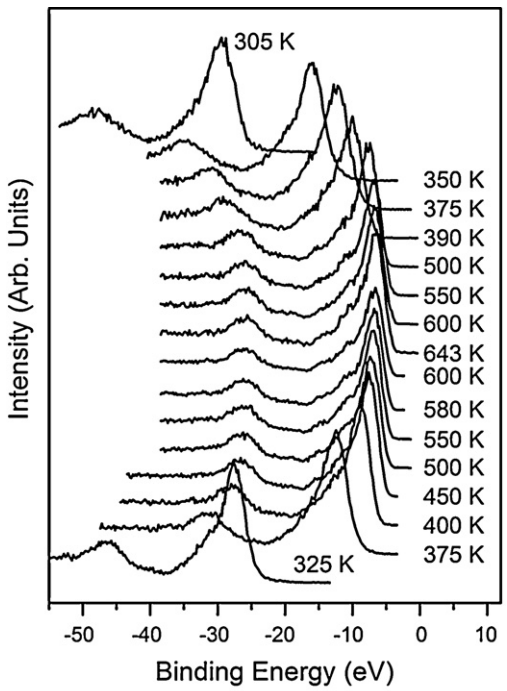

Fig. 3. The photoemission spectra from Cu doped $Li_2B_4O_7(1\,0\,0)$ surface for a succession of temperatures in a heating-cooling cycle (from bottom to top). The photoemission spectra were taken at a photon energy of 90 eV with electrons collected along the surface normal.

$Li_2B_4O_7(1\,0\,0)$ surface over the nominally undoped $Li_2B_4O_7(1\,0\,0)$ and $Li_2B_4O_7(1\,1\,0)$ surfaces is consistent with the unoccupied density of states that tails off towards the Fermi level, indicating a persistent presence of donor states. This may well be due to the Cu doping.

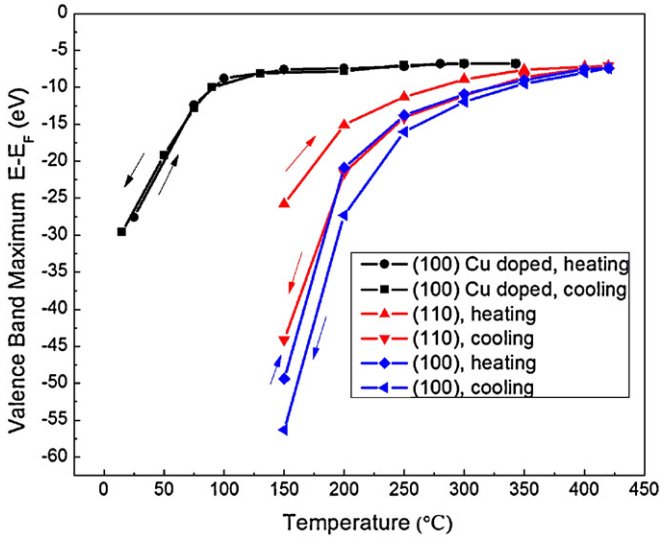

Fig. 4. Photovoltaic charging of $Li_2B_4O_7(1\,1\,0)$ (red), $Li_2B_4O_7(1\,0\,0)$ (blue) and Cu doped $Li_2B_4O_7(1\,0\,0)$ or $Li_{1.998}Cu_{0.002}B_4O_7(1\,0\,0)$ (black) as measured from the position of the valence band maximum. Position of the apparent valence band maximum for both the $(1\,1\,0)$ and $(1\,0\,0)$ surfaces of undoped $Li_2B_4O_7$, as well as Cu doped $Li_2B_4O_7(1\,0\,0)$, were taken, as in Fig. 3, with both heating and cooling and the shifts in the valence band maximum recorded in terms of the apparent binding energy with respect to the Femi level $E - E_F$. The data was obtained from photoemission spectra taken at a photon energy of 90 eV, with the photoelectrons collected normal to the surface.

Below 500 K, the photo-voltaic charging for the undoped $Li_2B_4O_7(1\,0\,0)$ and $Li_2B_4O_7(1\,1\,0)$ surfaces is both temperature and time dependent, particularly at the $(1\,1\,0)$ surface. There is hysteresis in the photovoltaic charging observed in photoemission. Although the photovoltaic charging is greater for the $(1\,0\,0)$ surface than the $(1\,1\,0)$ surface, the hysteresis is larger for the $(1\,1\,0)$ surface, as determined from the apparent position of the valence band maximum plotted in Fig. 4 [20,31]. This hysteresis in the surface photovoltaic charging, as measured by the valence band maximum, is consistent with the observation of a pyroelectric current along the $(1\,1\,0)$ direction at the much lower temperatures of 70–250 K, as discussed elsewhere [19–20]. It is interesting to note that the surface photovoltaic charging for both Cu doped and undoped $Li_2B_4O_7(1\,0\,0)$ surfaces exhibits a generally similar dependence on temperature but is shifted in temperature by 130°. The trend in the temperature dependence for the doped and undoped $Li_2B_4O_7(1\,0\,0)$ surfaces, seen in Fig. 4, differs from the temperature dependence seen for the undoped $Li_2B_4O_7(1\,1\,0)$ surfaces. This suggests that it is the carrier concentration that is altered with Cu doping, not the surface termination.

6. Summary

We find that Cu acts as a donor state in the region of the surface, likely occupying the Li sites substitutionally in $Li_2B_4O_7$ lattice. While remaining an insulator with the Cu dopants added, the surface photovoltaic charging is much diminished and surface charging in photoemission is minimal at much lower temperatures, well below 475 K, as opposed to the necessary 600–700 K needed to suppress surface charging for the undoped materials. Unlike the undoped materials, for the Cu doped $Li_2B_4O_7(1\,0\,0)$ surface, the hysteresis in the photovoltaic charging observed in photoemission is suppressed. Complications of surface termination are a concern, but no evidence of band bending in the vicinity of the surface was found in either photoemission or inverse photoemission. A definite assertion that the copper impurities act as a donor state within the bulk $Li_2B_4O_7$ crystal lattice requires bulk transport measurements. The possibility that Cu^{1+} defect impurities in the lithium site act as a hole trap in the bulk crystal cannot be excluded by the data presented here. The contributions of hole conductivity are likely to be much smaller when compared to electron transport. The evidence tends to support electron transport as the dominant conductivity mechanism: the Fermi level is observed to be placed closer to the conduction band edge, as seen in the combined photoemission and inverse photoemission, and the hole mass is likely very heavy compared to the electron mass [18]. Thus it is likely that the surface conductivity is dominated by electron transport, whose carrier lifetime and concentration may increase with Cu doping at the surface [20,24].

Acknowledgments

This work was supported by the Defense Threat Reduction Agency (Grant No. HDTRA1-07-1-0008 and BRBAA08-I-2-0128), the NSF "QSPINS" MRSEC (DMR-0820521) at UNL. The authors would like to thank Shan Yang (杨山) and L.E. Halliburton for technical support and insights into the EPR spectra. The views expressed in this article are those of the authors and do not reflect the official policy or position of the Air Force, Department of Defense or the U.S. Government.

References

[1] A.N. Caruso, R.B. Billa, S. Balaz, J.I. Brand, P.A. Dowben, J. Phys. Condensed Matter 16 (2004) L139.

[2] B.W. Robertson, S. Adenwalla, A. Harken, P. Welsch, J.I. Brand, P.A. Dowben, J.P. Claassen, Appl. Phys. Lett. 80 (2002) 3644.
[3] B.W. Robertson, S. Adenwalla, A. Harken, P. Welsch, J.I. Brand, J.P. Claassen, N.M. Boag, and P.A. Dowben, Adv. Neutron Scatt. Instrum., Anderson, I.S.; Guérard, B., Eds. Proc. SPIE 4785 (2002) 226.
[4] S. Adenwalla, R. Billa, J.I. Brand, E. Day, M.J. Diaz, A. Harken, A.S. McMullen-Gunn, R. Padmanabhan, B.W. Robertson, Penetrating Radiation Systems and Applications V, in: Proceedings SPIE, vol. 5199, 2003, p. 70.
[5] K. Osberg, N. Schemm, S. Balkir, J.I. Brand, S. Hallbeck, P. Dowben, M.W. Hoffman, IEEE Sens. J. 6 (2006) 1531.
[6] A.N. Caruso, P.A. Dowben, S. Balkir, N. Schemm, K. Osberg, R.W. Fairchild, O.B. Flores, S. Balaz, A.D. Harken, B.W. Robertson, J.I. Brand, Mater. Sci. Eng. B 135 (2006) 129.
[7] E. Day, M.J. Diaz, S. Adenwalla, J. Phys. D: Appl. Phys. 39 (2006) 2920.
[8] D.S. McGregor, T.C. Unruh, W.J. McNeil, Nucl. Instrum. Methods Phys. Res. A 591 (2008) 530.
[9] J. Uher, S. Pospisil, V. Linhart, M. Schieber, Appl. Phys. Lett. 90 (2007) 124101.
[10] Y. Kumashiro, J. Mater. Res. 5 (1990) 2933.
[11] Y. Kumashiro, J. Solid State Chem. 133 (1997) 314.
[12] Sangeeta, K. Chennakesavulu, D.G. Deai, S.C. Sabharwal, M. Alex, M.D. Ghodgaonkar, Nucl. Instrum. Methods Phys. Res. A 571 (2007) 699.
[13] Ya.B. Burak, V.T. Adamiv, I.M. Teslyuk, V.M. Shevel, Radiat. Meas. 38 (2004) 681.
[14] M.M. Islam, V.V. Maslyuk, T. Bredow, C. Minot, J. Phys. Chem. B 109 (2005) 13597.
[15] V.T. Adamiv, Ya.B. Burak, I.V. Kityk, J. Kasperczyk, R. Smok, M. Czerwinski, Opt. Mater. 8 (1997) 207.
[16] Ya.V. Burak, Ya.O. Dovgyi, I.V. Kityk, Solid State Phys 31 (1989) 275.
[17] Ya.V. Burak, V.T. Adamiv, O.T. Antonyak, S.Z. Malynych, M.S. Pidzyrailo, I.M. Teslyuk, Ukr. J. Phys. 50 (2005) 1153.
[18] D. Wooten, I. Ketsman, J. Xiao, Ya.B. Losovyj, J. Petrosky, J. McClory, Ya.V. Burak, V.T. Adamiv, J.M. Brown, P.A. Dowben, Eur. J. Phys.: Appl. Phys. (2010), doi:10.1051/epjap/2010160.
[19] I. Ketsman, D. Wooten, J. Xiao, Ya.B. Losovyj, Ya.V. Burak, V.T. Adamiv, A. Sokolov, J. Petrosky, J. McClory, P.A. Dowben, Phys. Lett. A 374 (2010) 891–895.
[20] V.T. Adamiv, Ya.V. Burak, D. Wooten, J. McClory, J. Petrosky, I. Ketsman, J. Xiao, Ya.B. Losovyj, P.A. Dowben, Materials 3 (2010) 4550–4579, doi:10.3390/ma3094550.
[21] A.S. Bhalla, L.E. Cross, R.W. Whatmore, Jpn. J. Appl. Phys. 24 (Suppl 24-2) (1985) 727.
[22] Ya.V. Burak, J. Phys. Stud. 2 (1998) 62.
[23] P.A. Dowben, A. Miller (Eds.), Surface Segregation Phenomena, CRC Press, Boca Raton, Florida, 1990.
[24] V.T. Adamiv, V.P. Savchyn, P.V. Savchyn, I.M. Teslyuk, Ya.V. Burak, Funct. Mater. 16 (2009) 247–252.
[25] O.T. Antonyak, V.T. Adamiv, Ya.V. Burak, I.M. Teslyuk, Funct. Mater. 9 (2002) 1.
[26] Ya.B. Losovyj, I. Ketsman, E. Morikawa, Z. Wang, J. Tang, P.A. Dowben, Nucl. Instrum. Methods Phys. Res. A 582 (2007) 264.
[27] Ya.B. Losovyj, D. Wooten, J.C. Santana, J.M. An, K.D. Belashchenko, N. Lozova, J. Petrosky, A. Sokolov, J. Tang, W. Wang, N. Arulsamy, P.A. Dowben, J. Phys. Condensed Matter 21 (2009) 045602.
[28] P.A. Dowben, D. LaGraffe, M. Onellion, J. Phys. Condensed Matter 1 (1989) 6571.
[29] D.N. McIlroy, J. Zhang, P.A. Dowben, D. Heskett, Mater. Sci. Eng. A 217/218 (1996) 64.
[30] C.N. Borca, T. Komesu, P.A. Dowben, J. Electron. Spectrosc. Relat. Phenom. 122 (2002) 259.
[31] D. Wooten, I. Ketsman, Jie Xiao, Ya. B. Losovyj, J. Petrosky, J. McClory, Ya.V. Burak, V.T. Adamiv, P.A. Dowben, Physica B 405 (2010) 461–464.
[32] I.N. Yakovkin, P.A. Dowben, Surf. Rev. Lett. 14 (2007) 481.
[33] J. Häfner, J. Phys. Condensed Matter 22 (2010) 384205.
[34] S. Kümmel, L. Kronik, Rev. Mod. Phys. 80 (2008) 3.
[35] F. Bechstedt, F. Fuchs, G. Kresse, Phys. Status Solidi B 246 (2009) 1877.
[36] T. Stein, L. Kronik, R. Baer, J. Am. Chem. Soc. 131 (2009) 2818.
[37] M.-S. Liao, Y. Lu, S. Scheiner, J. Comput. Chem. 24 (2003) 623.
[38] J.E. Ortega, F.J. Himpsel, D. Li, P.A. Dowben, Solid State Commun. 91 (1994) 807.
[39] M.W. Swinney, J.W. McClory, J.C. Petrosky, S. Yang, A.T. Brant, V.T. Adamiv, Ya.V. Burak, P.A. Dowben, L.E. Halliburton, J. Appl. Phys. 107 (2010) 113715.
[40] C. Corradi, V. Nagirnyi, A. Kotlov, A. Watterich, M. Kirm, K. Polgar, A. Hofstaetter, M. Meyer, J. Phys.: Condensed Matter 20 (2008) 025216.
[41] D. Piwowarska, S.M. Kaczmarek, M. Berkowski, I. Stefaniuk, J. Cryst. Growth 291 (2006) 123.
[42] D. Podgorska, S.M. Kaczmarek, W. Drozdowski, M. Wabia, M. Kwasny, S. Warchol, V.M. Rizak, Mol. Phys. Rep. 39 (2004) 199.
[43] B.M. Gunda, P.P. Puga, A.M. Solomon, M.I. Golovey, Ukr. Fiz. Zh. 45 (2000) 337.
[44] M. Ishii, Y. Kuvano, T. Asai, N. Senguttuvan, T. Hayashi, M. Kobayashi, T. Oku, K. Sakai, T. Adachi, H.M. Shimizu, J. Suzuki, J. Cryst. Growth 257 (2003) 169.
[45] K.S. Park, J.K. Ahn, D.J. Kim, H.K. Kim, Y.H. Hwang, D.S. Kim, M.H. Park, Y. Park, J.J. Yoon, J.Y. Leem, J. Cryst. Growth 249 (2003) 483.
[46] N. Senguttuvan, M. Ishii, M. Shimoyama, M. Kobayashi, N. Tsutsui, M. Nikl, M. Dusek, H.M. Shimizu, T. Oku, T. Adachi, K. Sakai, J. Suzuki, Nucl. Instrum. Methods A 486 (2002) 264.
[47] V.M. Holovey, V.I. Sidney, V.I. Lyamayev, P.P. Puga, J. Lumin. 126 (2007) 408.
[48] W.H. Brattain, J. Bardeen, Bell Syst. Technol. J. 32 (1953) 1–41.
[49] D.K. Schroder, Meas. Sci. Technol. 12 (2001) R16–R31.
[50] J.E. Demuth, W.J. Thompson, N.J. DiNardo, R. Imbihl, Phys. Rev. Lett. 56 (1986) 1408–1411.
[51] M. Alonso, R. Cimino, K. Horn, Phys. Rev. Lett. 64 (1990) 1947–1950.
[52] K. Stiles, A. Kahn, Phys. Rev. Lett. 60 (1988) 440–443.